Vacuum ultraviolet-ultraviolet and x-ray excited luminescence properties of $Ba_3Gd(BO_3)_3:Ce^{3+}$

Bing Han, Hong-bin Liang,[a] Hui-hong Lin, Jiu-ping Zhong, and Qiang Su
MOE Laboratory of Bioinorganic and Synthetic Chemistry, State Key Laboratory of Optoelectronic Materials and Technologies, School of Chemistry and Chemical Engineering, Sun Yat-Sen University, Guangzhou 510275, China

Pieter Dorenbos and M. Danang Birowosuto
Faculty of Applied Sciences, Delft University of Technology, Mekelweg 15, 2629 JB Delft, The Netherlands

Guo-bin Zhang and Yi-bing Fu
National Synchrotron Radiation Laboratory, University of Science and Technology of China, Hefei 230026, People's Republic of China

(Received 31 January 2007; accepted 16 April 2007; published online 13 June 2007)

The phosphors $Ba_3Gd(BO_3)_3:Ce^{3+}$ were prepared by a solid-state reaction technique at high temperature. The vacuum ultraviolet-ultraviolet and visible spectroscopic properties of the phosphors together with decay time curves are investigated and discussed. The spectroscopic properties are explained by occupancy of Ce^{3+} at two different Gd sites in the host lattice. The x-ray excited emission spectra of $Ba_3Gd(BO_3)_3:Ce^{3+}$ were studied and the number of photons emitted per unit of absorbed x-ray energy was calculated. The yield is rather poor and $Ba_3Gd(BO_3)_3:Ce^{3+}$ appears not a suitable x-ray phosphor. © *2007 American Institute of Physics*.
[DOI: 10.1063/1.2743826]

I. INTRODUCTION

Research on Ce^{3+} ion doped materials has been of importance for many decades for basic research and for potential industrial applications. Ce^{3+} is an ion with ground state configuration $[Xe]4f^15d^0$ in which only one electron occupies the $4f$ orbital and the $5d$ state is empty. It is a typical rare-earth ion with $4f$-$5d$ transitions that is parity allowed and thus results in broad bands in absorption and excitation spectra. The $4f$-$5d$ transitions of Ce^{3+} appear in a wavelength range that depends strongly on the type of host lattice. The transition energies provide important information on the $5d$ crystal field splitting, the $5d$ centroid, and the Stokes shift of $5d$ states from which the site symmetry of the lanthanide in the host lattices can be deduced.[1–3] Moreover, some Ce^{3+}-doped materials such as $Y_3Al_5O_{12}:Ce^{3+}$, $LaPO_4:Ce^{3+}$, Tb^{3+}, $SrAl_{12}O_{19}:Ce^{3+}$, $Lu_2SiO_5:Ce^{3+}$, and $LuAlO_3:Ce^{3+}$ are applied as phosphors in lighting and display, and as scintillators for medical imaging or precision calorimetry in high energy physics.[4–6] From the standpoint of application, the research on Ce^{3+}-doped materials continues with the aim to develop some phosphors and inorganic scintillators with much better quality than the existing ones.

Borate compounds, as a large class of host lattices for luminescent ions, are of interest because of their easy synthesis, good chemical stability, and low material cost. Vacuum ultraviolet (vuv, with wavelength $\lambda < 200$ nm and energy $E > 50\,000$ cm^{-1}) phosphors must have the ability to absorb vuv light efficiently combined with high energy-transfer efficiency from the host lattice to activator ions. Most borates satisfy these conditions, and they exhibit a proper width of band gap. In this work the compound $Ba_3Gd(BO_3)_3$ is chosen as the host lattice for Ce^{3+}. The Gd^{3+} ions can play two different roles. Energy can be transferred over the Gd sublattice from the sensitizer, which can be the host lattice itself, to the activator, and in addition Gd^{3+} is a well known quantum-cutting ion.[7,8] The syntheses of compounds $M_3Ln(BO_3)_3$ (M=Sr, Ba and Ln=La–Lu, Sc, Y) have been reported in recent years,[9–12] but the spectroscopic properties of Ce^{3+} ion-activated $Ba_3Gd(BO_3)_3$ have not been reported yet.

In this work, the luminescence properties of Ce^{3+}-doped barium gadolinium borate $Ba_3Gd(BO_3)_3:Ce^{3+}$ under vuv, uv, and x-ray excitations are reported.

II. EXPERIMENT

All powder samples were prepared using a high-temperature solid-state reaction technique. For preparation of the pure host compound $Ba_3Gd(BO_3)_3$ and the Ce^{3+}-doped samples $Ba_3Gd_{1-x}Ce_x(BO_3)_3$ (x=0.01, 0.02, 0.04, 0.06, 0.08, and 0.10), analytical reagent (AR) grade $BaCO_3$, H_3BO_3, Gd_2O_3 (99.99%), and CeO_2 (99.9%) were employed as reactants. A stoichiometric mixture with 3 mol % excess H_3BO_3, to compensate for the evaporation at high temperature, was ground thoroughly in an agate mortar and preheated at 700 °C in a muffle furnace. After ground again, the samples were fired at 1100 °C in reducing CO atmosphere for the Ce^{3+}-doped samples or in air for the undoped host compound, and then cooled down to room temperature (RT).

In order to interpret the spectroscopic properties and clarify the structure of $Ba_3Gd(BO_3)_3$, four other samples, i.e., $Ba_3Gd_{0.94}Eu_{0.06}(BO_3)_3$, $Ba_3Gd_{0.96}Sm_{0.04}(BO_3)_3$, low temperature phase $Ba_3Y(BO_3)_3$ [L-$Ba_3Y(BO_3)_3$],[13,14] and high-temperature phase $Ba_3Y(BO_3)_3$ [H-$Ba_3Y(BO_3)_3$] (Refs.

[a]Author to whom correspondence should be addressed; electronic mail: cesbin@mail.sysu.edu.cn

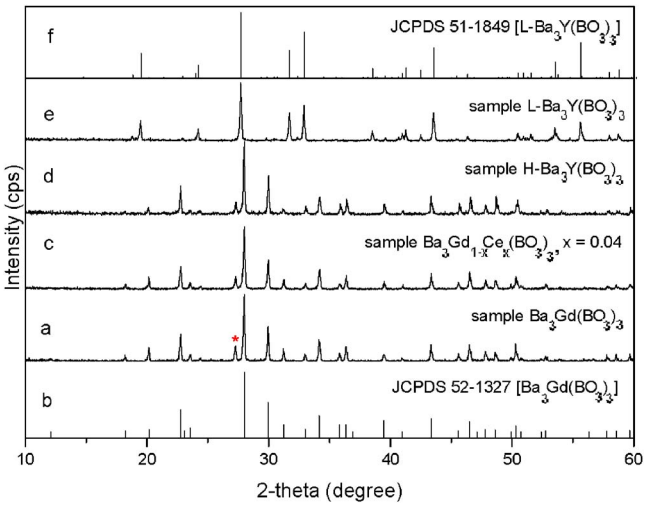

FIG. 1. (Color online) The XRD patterns for samples $Ba_3Gd(BO_3)_3$, $Ba_3Gd_{1-x}Ce_x(BO_3)_3$ (x=0.04), H-$Ba_3Y(BO_3)_3$, and L-$Ba_3Y(BO_3)_3$.

15 and 16) were also prepared. The preparation process for the Sm^{3+}- and Eu^{3+}-doped samples are the same as described above for the undoped compound in air ambient. Sm^{3+} and Eu^{3+} ions are provided by Sm_2O_3 (99.99%) and Eu_2O_3 (99.99%), respectively. For preparation of the low and high-temperature phases of $Ba_3Y(BO_3)_3$, Y_2O_3 (99.999%) was used as a reactant and the heating temperatures in the final step were 1100 and 1200 °C, respectively.

To characterize the phase purity and structure of the samples, a powder x-ray diffraction (XRD) analysis was carried out with Cu $K\alpha$ (λ=1.5405 Å) radiation on a Rigaku D/max 2200 vpc x-ray diffractometer.

The uv excitation and emission spectra of the phosphors were recorded with a Jobin Yvon FL3-21 spectrofluorometer at room temperature. The luminescence decay curves were measured at an Edinburgh FLS 920 combined fluorescence lifetime and steady-state spectrometer. The vuv excitation and corresponding luminescent spectra were measured at the vuv spectroscopy experimental station on beamline U24 of the National Synchrotron Radiation Laboratory. The x-ray excited emission spectra were recorded with an x-ray tube with Cu anode operating at 35 kV and 25 mA. Further measurement details can be found in our previous work.[17,18]

III. RESULTS AND DISCUSSION

A. XRD patterns and the structure of $Ba_3Gd(BO_3)_3$

The XRD pattern of sample $Ba_3Gd(BO_3)_3$ is displayed in Fig. 1(a). It agrees with the JCPDS standard card in Fig. 1(b) except for a reflection around 27.3° that is marked by red asterisk (*) in the diffraction pattern. We think that the reflection might also be attributable to the sample $Ba_3Gd(BO_3)_3$, because this reflection occurs in the JCPDS standard cards of other isomorphic compounds such as $Ba_3Nd(BO_3)_3$, $Ba_3Sm(BO_3)_3$, $Ba_3Eu(BO_3)_3$, $Ba_3Tb(BO_3)_3$, and $Ba_3Dy(BO_3)_3$.[26] In addition, to exclude the probability of impurity for the reflection, we searched and compared all JCPDS standard cards of the raw materials and the Gd/Ba/B/O-containing binary or ternary compounds, and it was found that above reflection could not be attributed to any impurity phase. All these works evidence that the reflection around 27.3° might be attributed to the sample $Ba_3Gd(BO_3)_3$. The XRD patterns for samples $Ba_3Gd_{1-x}Ce_x(BO_3)_3$ with different doping concentrations (x) and $Ba_3Gd_{0.94}Eu_{0.06}(BO_3)_3$, $Ba_3Gd_{0.96}Sm_{0.04}(BO_3)_3$ also agree with Fig. 1(b). The diffractogram of $Ba_3Gd_{0.96}Ce_{0.04}(BO_3)_3$ as an example is exhibited in Fig. 1(c). It shows that the structure of $Ba_3Gd(BO_3)_3$ is maintained for the doping concentration range that we investigated. The dopant Ce^{3+} is slightly larger than Gd^{3+} but it will not distort the crystal lattice of $Ba_3Gd(BO_3)_3$ too seriously and is expected to replace Gd^{3+} ions.

In the last decade, several reports on the crystal structure of $Ba_3Ln(BO_3)_3$ (Ln=La–Lu, Y, Sc) compounds have appeared.[9–12] They crystallize in two different structures. For Ln=La–Tb, they are in the trigonal system (I) with space group $R\bar{3}$. For Ln=Dy–Lu, Y, Sc, the compounds can exist in both the trigonal system (I) with space group $R\bar{3}$ and the hexagonal system (II) with space group $P6_3cm$, depending on the formation temperature. When $Ba_3Ln(BO_3)_3$ (Ln=Dy, Ho, Er, and Y) with structure (II) synthesized at temperature T_{II} is heated to temperature T_I ($T_I > T_{II}$), its structure will change from (II) to (I). Therefore, the trigonal structure (I) can be regarded as a high-temperature phase and the hexagonal structure (II) as a low-temperature phase.

For two different structural $Ba_3Ln(BO_3)_3$ and their conversions, the compound $Ba_3Y(BO_3)_3$ is a typical example. When the low-temperature phase $Ba_3Y(BO_3)_3$ [L-$Ba_3Y(BO_3)_3$] with structure (II) is heated above 1148 °C it changes into the high-temperature phase $Ba_3Y(BO_3)_3$ [H-$Ba_3Y(BO_3)_3$] with structure (I). The crystal structure of both phases was reported in detail.[13–16] Although XRD data were reported[11] for $Ba_3Gd(BO_3)_3$, its detailed structure has not been depicted so far.

In order to better interpret the spectroscopic properties of $Ba_3Gd(BO_3)_3$, we prepared H-$Ba_3Y(BO_3)_3$ and L-$Ba_3Y(BO_3)_3$. The XRD patterns of these two Y-based samples are shown in Figs. 1(d) and 1(e). The XRD patterns of sample L-$Ba_3Y(BO_3)_3$ in Fig. 1(e) agree with the JCPDS standard card in Fig. 1(f). We did not find the XRD pattern of H-$Ba_3Y(BO_3)_3$ in the JCPDS database PDF2. It can be seen that the XRD pattern of $Ba_3Gd(BO_3)_3$ in Fig. 1(a) agrees with that of H-$Ba_3Y(BO_3)_3$ in Fig. 1(d) which is clearly different from that of L-$Ba_3Y(BO_3)_3$ in Fig. 1(e).

A detailed structure description of $Ba_3Gd(BO_3)_3$ was not found in literature. In this work we assume that $Ba_3Gd(BO_3)_3$ is isomorphic with H-$Ba_3Y(BO_3)_3$ for the following three reasons: (1) The powder XRD patterns of $Ba_3Gd(BO_3)_3$ and H-$Ba_3Y(BO_3)_3$ are similar, as shown in Fig. 1. (2) The ionic radii of Gd^{3+} [$R_{Gd(III)}$=93.8 pm] are close to that of Y^{3+} [$R_{Y(III)}$=90.0 pm] in sixfold coordination.[19] (3) It was found that the unit cell parameters [a=13.067(3) Å, c=9.552(3) Å, trigonal, $R\bar{3}$] of $Ba_3Gd(BO_3)_3$ are similar with that [a=13.028(2) Å, c=9.4992(2) Å, trigonal, $R\bar{3}$] of H-$Ba_3Y(BO_3)_3$.[11,15]

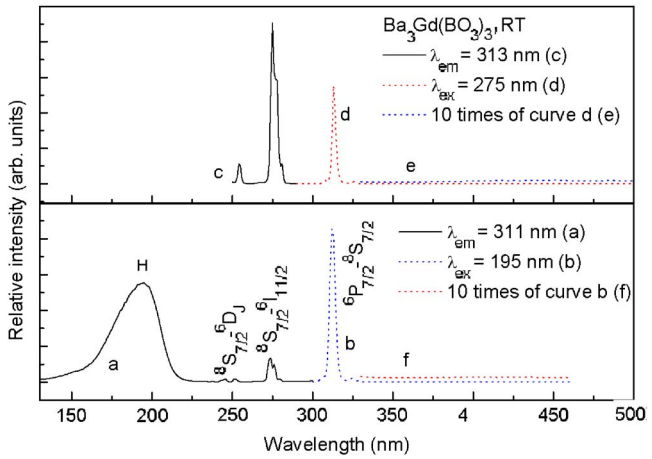

FIG. 2. (Color online) vuv excitation spectrum [curve (a)], vuv excited emission spectrum [curve (b)], uv excitation spectrum [curve (c)], and uv excited emission spectrum [curve (d)] of sample $Ba_3Gd(BO_3)_3$.

B. vuv-uv spectroscopic properties of $Ba_3Gd(BO_3)_3$

Figure 2 shows vuv-uv excitation and emission spectra of $Ba_3Gd(BO_3)_3$. In vuv excitation curve (a), the $^8S_{7/2}$-^6D_j transitions around 250 nm and the $^8S_{7/2}$-$^6I_{11/2}$ transition at 274 nm of Gd^{3+} are observed. These excitation lines are found in the uv excitation spectrum (c) also. Curves (b) and (d) display the emission spectra under vuv-uv excitation. As shown in curve (d), the Gd^{3+} $^6P_{7/2}$-$^8S_{7/2}$ emission at 313 nm is observed when Gd^{3+} is excited. This emission is also found in curve (b) upon 195 nm vuv excitation. The broad excitation band at about 195 nm in curve (a) is attributed to the host absorption as discussed below. Apparently the host lattice transfers excitation energy to Gd^{3+}. In addition, we note that for the low-temperature phase $Ba_3Y(BO_3)_3$ a host emission at about 415 nm was observed under x-ray excitation.[20] Such emission was not observed in $Ba_3Gd(BO_3)_3$ under vuv-uv excitation even after ten times enlarging the emission spectra, as shown in Figs. 2(e) and 2(f).

In the vuv excitation spectrum (a), a broad band (marked as *H*) with a maximum at 195 nm is observed. From general considerations,[17] the absorption of $Ba_3Gd(BO_3)_3$ in the vuv range may be due to four types of electronic excitation processes: (1) The intraconfiguration $4f^7$-$4f^7$ transitions of Gd^{3+}.[7] (2) The intraconfiguration $4f^7$-$4f^6 5d$ transitions of Gd^{3+}. (3) Charge transfer (CT) transitions from O^{2-} ligand atoms to Gd^{3+}.[21] (4) The intramolecular absorption of the BO_3^{3-} anion in $Ba_3Gd(BO_3)_3$.

It is well known that the $4f$-$4f$ transitions of lanthanide ions are narrow linelike, and the broad band *H* can therefore not be assigned to $4f^7$-$4f^7$ transitions of Gd^{3+}. The $4f^7$-$4f^6 5d$ transitions are also improbable because Gd^{3+} has a half-filled $4f$ shell and the lowest energy of the $4f^7$-$4f^6 5d$ transitions is expected at higher energy region in oxide compounds. Further in this work we will estimate the location of the $4f^7$-$4f^6 5d$ transition with the lowest energy of Gd^{3+} at around 135 nm from data on that of Ce^{3+}.

The CT energy for the O^{2-}–Gd^{3+} transfer can be estimated from the CT energy of other rare-earth ions such as Sm^{3+} and Eu^{3+} in the same host lattice. Figure 3 shows the uv excitation spectra for $Ba_3Gd(BO_3)_3$:$0.06Eu^{3+}$ and $Ba_3Gd(BO_3)_3$:$0.04Sm^{3+}$. We obtained the uv excitation spectrum (b) of sample $Ba_3Gd(BO_3)_3$:$0.06Eu^{3+}$ by monitoring the $^5D_0$-$^7F_2$ emission of Eu^{3+} at 612 nm, and the uv excitation spectrum (a) of sample $Ba_3Gd(BO_3)_3$:$0.04Sm^{3+}$ by monitoring the $^4G_{5/2}$-$^6H_{7/2}$ emission of Sm^{3+} at 602 nm. In spectrum (a), a broad band *A* with a maximum at 227 nm is observed which we attribute to the charge transition band (CTB) of Sm^{3+}. The lines around 252, 273, and 312 nm are from $4f^7$-$4f^7$ transitions of Gd^{3+} that are also observed in Fig. 2. The features in spectrum (a) at wavelengths longer than 320 nm are from $4f^5$-$4f^5$ transitions of Sm^{3+}.

Spectrum (b) shows a broad band *B* with maximum at 275 nm that we attribute to the CTB of Eu^{3+}. The width and the location are typical for the Eu^{3+} CTB in oxide compounds. The strong dipole allowed CT excitation band over-

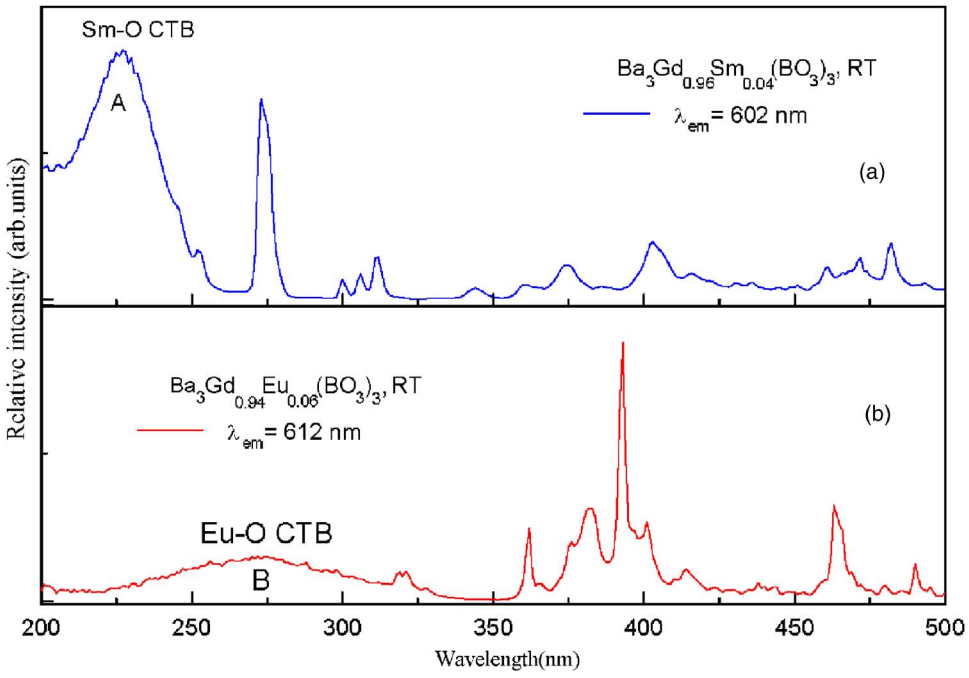

FIG. 3. (Color online) uv excitation spectrum [curve (a)] of sample $Ba_3Gd(BO_3)_3$:$0.04Sm^{3+}$ and uv excitation spectrum [curve (b)] of sample $Ba_3Gd(BO_3)_3$:$0.06Eu^{3+}$.

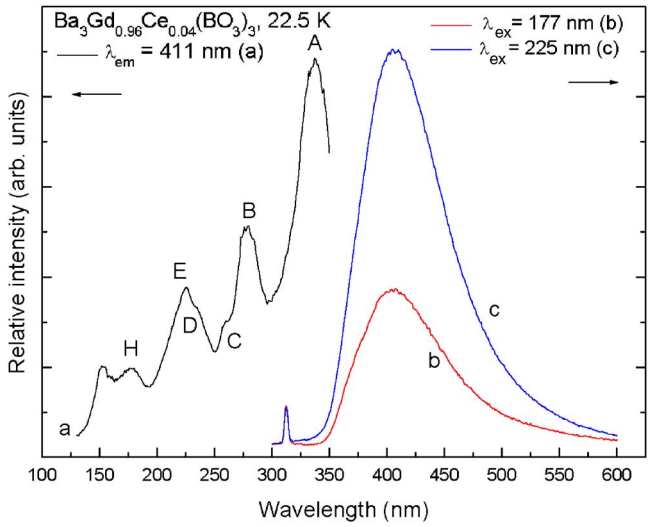

FIG. 4. (Color online) The vuv excitation and emission spectra for samples $Ba_3Gd_{0.96}Ce_{0.04}(BO_3)_3$ at 22.5 K.

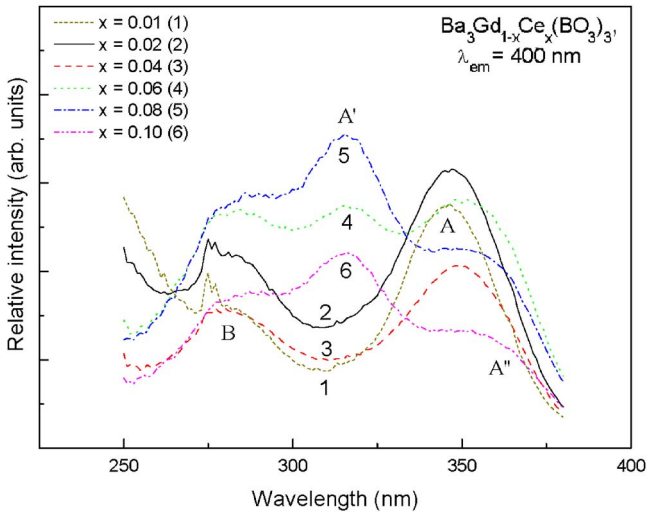

FIG. 5. (Color online) The uv excitation spectra under 400 nm emission for samples $Ba_3Gd_{1-x}Ce_x(BO_3)_3$ with different doping concentrations at RT.

laps the weak forbidden $4f^7$-$4f^7$ excitation lines of Gd^{3+} which are not observed in the spectrum (b). The transitions between 320 and 500 nm in spectrum (b) are attributed to the $4f^6$-$4f^6$ transitions of Eu^{3+}.

The energies of CT excitation for different rare-earth ions in the same host lattice were systematically analyzed by one of us.[22] In that work, it was found that the excitation energy of the $Sm^{3+} \leftarrow O^{2-}$ CT band is always about 1.16 eV higher than that of the $Eu^{3+} \leftarrow O^{2-}$ CT band. We therefore predict that the $Sm^{3+} \leftarrow O^{2-}$ CT band should be located at around 5.67 eV (219 nm). This is at somewhat higher energy than the observed band at 5.44 eV (227 nm) in Fig. 3(a). Possibly the $Sm^{3+} \leftarrow O^{2-}$ CT band in Fig. 3(a) is deformed on the high energy side by competing excitation of band *H* of the pure compound, see Fig. 2(a). Although a $Gd^{3+} \leftarrow O^{2-}$ CT band has never been observed in a compound, its location should be at 4.32 eV higher than that of the $Eu^{3+} \leftarrow O^{2-}$ CT band.[22] We therefore expect the CT excitation of $Gd^{3+} \leftarrow O^{2-}$ at about 8.83 eV (140 nm) in $Ba_3Gd(BO_3)_3$. Clearly the band *H* in Fig. 2(a) cannot be attributed to the $Gd^{3+} \leftarrow O^{2-}$ CT band in $Ba_3Gd(BO_3)_3$.

Excluding $4f$-$4f$, $4f$-$5d$, and the $Gd^{3+} \leftarrow O^{2-}$ CT excitation as possible causes for band *H* in Fig. 2(a), a remaining cause can be the intramolecular absorption of BO_3^{3-} anions in $Ba_3Gd(BO_3)_3$. The maximum of the host-related excitation band at 195 nm appears, however, at lower energy than what is usually observed for borate compounds. It is at about 160 nm for $YAl_3(BO_3)_4$, 165 nm for $(Y,Gd)BO_3$, 170 nm for $SrAl_2B_2O_7$, and 190 nm for $BaZr(BO_3)_2$.[23,24] The true origin for host band *H* in $Ba_3Gd(BO_3)_3$ has not been therefore fully resolved yet.

C. Spectroscopic properties of $Ba_3Gd(BO_3)_3:Ce^{3+}$ in vuv-uv and visible range

1. Excitation spectra

Figure 4 shows the vuv excitation spectrum [curve (a)], the vuv excited emission spectrum [curve (b)], and the uv excited emission spectrum [curve (c)] of $Ba_3Gd_{0.96}Ce_{0.04}(BO_3)_3$ at 22.5 K. The bands below 200 nm in curve (a) are in the wavelength region where also host-related absorption bands were observed. At wavelengths above 200 nm we can clearly identify at least five broad bands, marked as *A* (338 nm), *B* (280 nm), *C* (260 nm), *D* (235 nm), and *E* (225 nm). The bands must be attributed to transitions from the $4f$ ground state to levels of the crystal field split $5d$ configuration of Ce^{3+}.

As mentioned in Sec. III A, we will discuss the spectroscopic features of Ce^{3+} in $Ba_3Gd(BO_3)_3$ by using the trigonal structure (I) of *H*-$Ba_3Y(BO_3)_3$ which was depicted in detail.[14] In *H*-$Ba_3Y(BO_3)_3$, two alternating nonequivalent Y atoms form one-dimensional chains bridged by the Ba atoms with BO_3 triangles that link Y(1) and Y(2), respectively. Both Y(1) and Y(2) occupy distorted octahedral sites with S_6 point symmetry. Y(1) ions are coordinated by six O(1) atoms whereas Y(2) ions are coordinated by six O(2) atoms. The Y(1)–O(1) bond length of 2.534(1) Å is much longer than that of Y(2)–O(2) which is only 2.235(8) Å. When we assume that $Ba_3Gd(BO_3)_3$ has the same trigonal structure (I) as *H*-$Ba_3Y(BO_3)_3$, then Ce^{3+} ions may occupy two nonequivalent Gd^{3+} lattice sites in $Ba_3Gd(BO_3)_3$.

To further analyze the excitation bands we prepared five samples of $Ba_3Gd_{1-x}Ce_x(BO_3)_3$ with $x=0.01$, 0.02, 0.06, 0.08, 0.10 and measured the uv excitation spectra of 400 nm emission together with that for $x=0.04$, as shown in Fig. 5. Four characteristics are observed: (1) There is a broad band at 280 nm for all samples that corresponds with band (*B*) in Fig. 4. The band overlaps the 275 nm $4f$-$4f$ transition of Gd^{3+}. Only for low doping concentration such as $x=0.01$ (curve 1) the Gd^{3+} excitation at 275 nm is clearly observed. (2) There is an excitation band (*A*) around 350 nm that corresponds with band (*A*) in Fig. 4. However, band (*A*) is around 338 nm in Fig. 4, while in Fig. 5 it has shifted by about 10 nm to the longer-wavelength region. We attribute this redshift to a different response of the instrumental setup between the vuv measurements in NSRL and the uv measurements in our laboratory. The wavelength region of 340–350 nm is at the edge of the sensitivity of the grating

and the photomultiplier tube (PMT) at NSRL. We regard the uv measurements as more reliable and the real location of band A is then at 347 nm as in Fig. 5. (3) One band, labeled as A', around 316 nm was found for the samples with high doping concentration such as $x=0.06$, 0.08, 0.10 in Fig. 5. The band is absent for the samples with low doping concentration. The intensity of band A' increases with increase of Ce^{3+} concentration. (4) We observe that band A shifts to longer-wavelength region with increase of Ce^{3+} concentration. This phenomenon can be observed clearly at concentrations where also band A' appears. Like band A', another band A'' seems to appear for the samples with high doping concentration, and the relative intensity of band A'' increases with increase of Ce^{3+} concentration. For example, band A'' in curves 5 ($x=0.08$) and 6 ($x=0.10$) is almost equally intense as band A.

The results in Fig. 5 clearly suggest that excitation bands A and B belong to one type of Ce site and bands A' and A'' to another type. Further assuming that the smallest Gd site provides the largest crystal field splitting and consequently the lowest energy $5d$ state, we attribute bands A'' and A' to two $4f$-$5d$ transitions with the lowest energy in Ce^{3+} at the smaller Gd(2) site. Bands A and B then belong to Ce at the larger Gd(1) site. The ionic radius of Gd^{3+} is 93.8 pm and that of Ce^{3+} is 101 pm in sixfold coordination.[19] The larger Ce^{3+} will therefore preferentially occupy the larger Gd(1) site at low Ce^{3+} concentration. When the Ce^{3+} concentration increases also the Gd(2) site starts to be occupied. These expectations are fully in accord with the observed features in Fig. 5.

2. Emission spectra

Figures 4(b) and 4(c) show the emission spectra under 177 nm vuv and 225 nm uv excitation at 22.5 K. A broad emission band is observed in both cases. When Ce^{3+} occupies only one lattice site, a doublet emission from the lowest $5d$ state to the $^2F_{5/2}$ and $^2F_{7/2}$ levels of the spin orbit split $4f$ ground state occurs. But when Ce^{3+} ions enters two different lattice sites, the emission will be more complex and four emission bands should be present in theory. In Fig. 4, we observe a rather broad emission band under both 177 and 225 nm excitations. The emission at 225 nm excitation is redrawn as curve (a) in Fig. 6 to further analyze the double site occupancy of Ce^{3+} in the host. The emission can be fitted well by a sum of four Gaussian functions with maxima at 386, 417, 465, and 511 nm shown as curves (c), (d), (e), and (f) in Fig. 6. Curve (b) in Fig. 6 gives the sum of the four curves which fits very well to the observed spectrum. The energy difference is 19.2×10^2 cm^{-1} for the doublet emissions at 386 and 417 nm, and 19.4×10^2 cm^{-1} for the doublet emissions at 465 and 511 nm, which equals the usual energy difference between the Ce^{3+} $^2F_J(J=7/2,5/2)$ states. We therefore assign the bands at 386 and 417 nm to the emission from one Ce^{3+} site and the bands at 467 and 511 nm to the emission from another Ce^{3+} site.

To further explain the results, we measured the excitation spectra of 380 nm (short-wavelength) emission and 520 nm (long-wavelength) emission. The spectra are displayed in Figs. 7(a) and 7(b). Those in Fig. 7(a) are similar

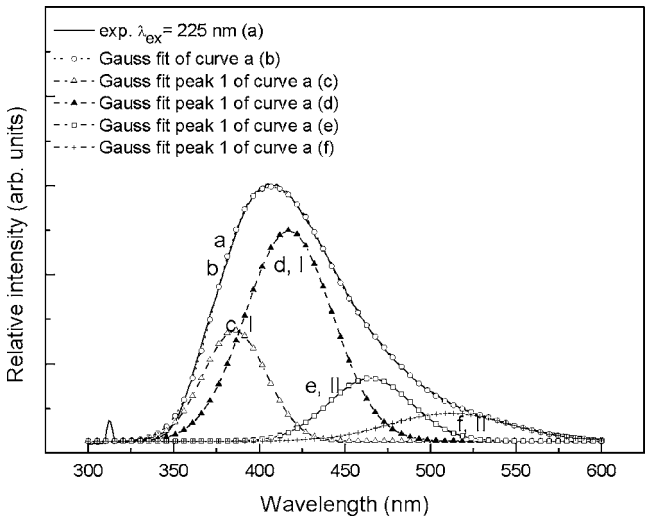

FIG. 6. The uv excited emission spectra for sample $Ba_3Gd_{0.96}Ce_{0.04}(BO_3)_3$ under 225 nm excitation at 22.5 K.

as the excitation spectra of 400 nm emission in Fig. 5. Monitoring the emission at 380 nm, band A at 347 nm is seen in all six curves of Fig. 7(a), but the relative intensity of this band is weak in the excitation curves (4), (5), and (6) for the samples with high doping concentration. This suggests that band A of the low Ce^{3+} concentration samples is related to the short-wavelength Ce^{3+} emission. It implies that the 386 and 417 nm doublet emissions are due to Ce^{3+} in the larger Gd(1) sites.

Figure 7(b) shows the excitation spectra of 520 nm (long-wavelength) emission. The weak band A at 347 nm in low Ce^{3+} concentration samples (curves 1–3) and the strong band A'' at 367 nm in high Ce^{3+} concentration samples (curves 4–6) are clearly observed. It reveals that the unresolved A'' band in Fig. 5 is actually located at about 367 nm. It also reveals that band A'' is related to the long-wavelength 465 and 511 nm doublet emissions and they are attributed to Ce^{3+} in the small Gd(2) sites.

Finally, Figs. 7(c)–7(e), show emission spectra excited at 316, 347, and 367 nm for 2% and 8% Ce^{3+}-doped samples. For the 2% Ce^{3+}-doped sample the Gd(1) site is preferentially occupied, and the emission is always at somewhat shorter wavelength than that for the 8% Ce^{3+}-doped sample.

Upon 316 or 367 nm excitation of Ce^{3+} in Gd(2) sites, the emission intensity of the 8% Ce^{3+}-doped sample is stronger than that of the 2% Ce^{3+}-doped sample. But upon 347 nm excitation of Ce^{3+} in Gd(1) sites, the sample with low doping concentration shows higher emission intensity. This is all consistent with our previous assignment that at low doping concentration Ce^{3+} prefers to occupy the large Gd(1) site and at high doping concentration also the small Gd(2) is occupied.

From the above data of excitation spectra and emission spectra, the values of Stokes shift for Ce^{3+} in Gd(1) are calculated to be 3.16×10^3 cm^{-1}, and 5.59×10^3 cm^{-1} for Ce^{3+} in Gd(2), which indicates that when Ce^{3+} enter into the smaller Gd(2) sublattice, it leads to a larger Stokes shift.

In a word, from above discussion we believe that Ce^{3+} might occupy two nonequivalent Gd^{3+} sites, the bands A and

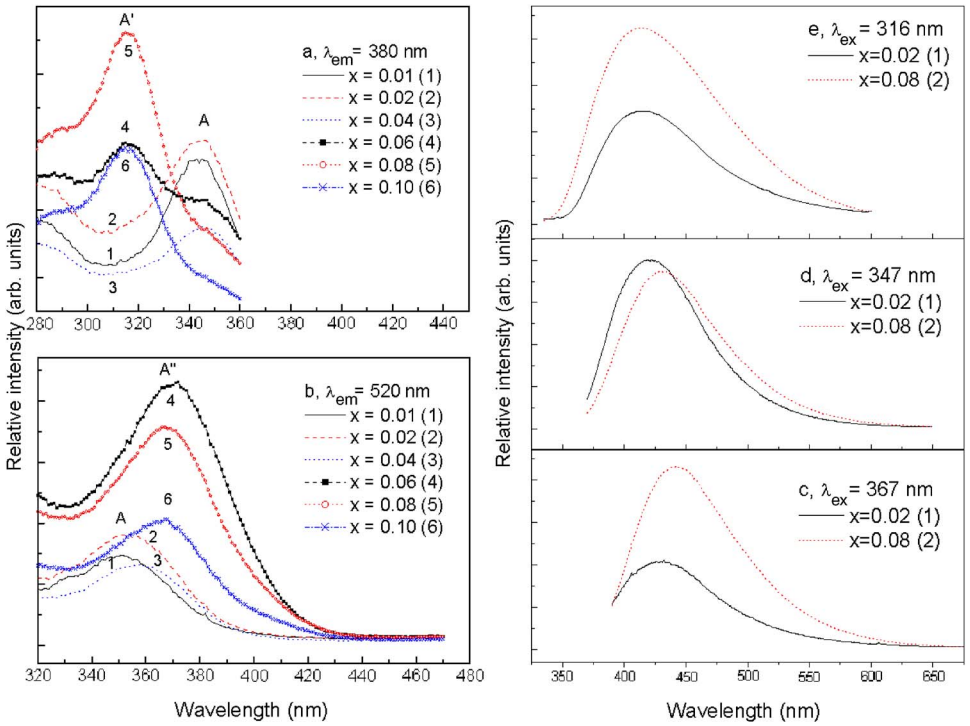

FIG. 7. (Color online) The uv excitation spectra under 380 and 520 nm emissions and the uv excitation emission spectra under 316, 347, and 367 nm excitations for samples $Ba_3Gd_{1-x}Ce_x(BO_3)_3$ with different doping concentrations at RT.

B belong to the absorption of Ce^{3+} in Gd(1) site, while the bands *A′* and *A″* the Gd(2) site. Ce^{3+} prefers to occupy the Gd(1) site at low Ce^{3+} concentration and the small Gd(2) is also occupied by Ce^{3+} at high Ce^{3+} concentration. The Ce^{3+} emissions from Gd(1) site are around 386 and 417 nm, whereas those from Gd(2) site are about 465 and 511 nm. Meanwhile, we are aware of that another possibility; the presence of few other phases in the samples may also change the spectra characteristics, though no any impurity phase was found in all samples according to a powder x-ray diffraction analysis, see Sec. III A above. Some other experiments, for instance, the high-resolution spectra of Eu^{3+} in the host lattice may be helpful to get a firm conclusion on this issue. The further work will be performed in the future.

From the energies of the lowest 5*d* states, we may also calculate the value for the so-called 5*d* redshift or crystal field depression $D(A)$ with the Dorenbos expression:[1]

$$E(\mathrm{Ln},A) = 49\,340\ \mathrm{cm}^{-1} - D(A) + \Delta E^{\mathrm{Ln,Ce}}. \quad (1)$$

Here, $E(\mathrm{Ln},A)$ is the 4*f*-5*d* energy difference in units of cm^{-1} of the lanthanide ion Ln^{3+} doped in compound *A*; 49 340 cm^{-1} is the lowest energy of the 4*f*-5*d* transition of Ce^{3+} as a free (gaseous) ion; $\Delta E^{\mathrm{Ln,Ce}}$ is defined as the difference in the lowest 4*f*-5*d* energy of Ln^{3+} with that of the

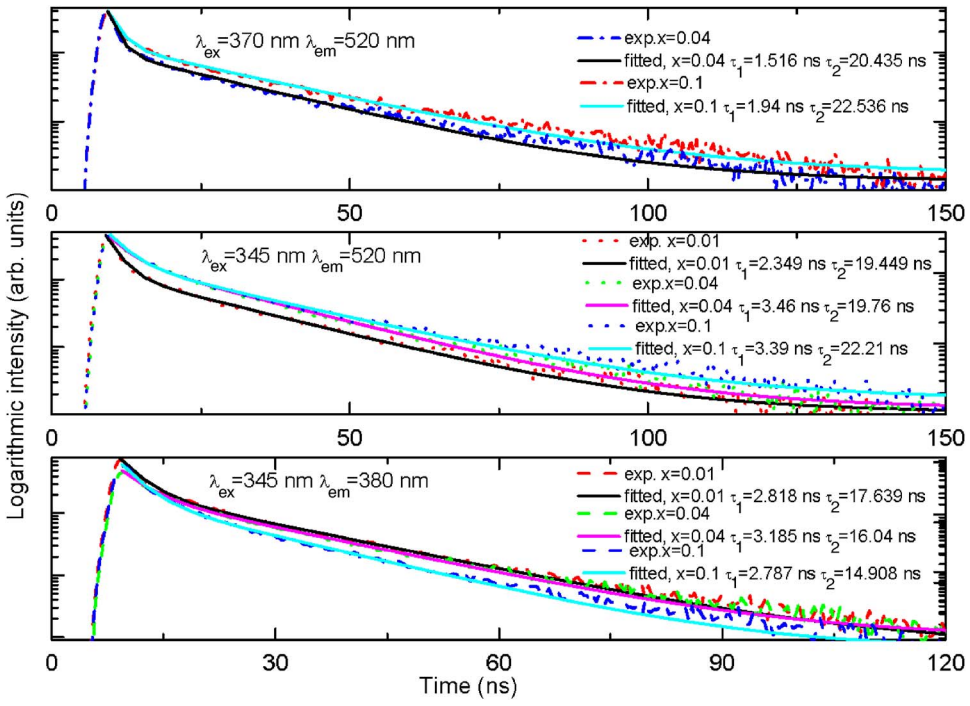

FIG. 8. (Color online) The decay curve of sample $Ba_3Gd_{1-x}Ce_x(BO_3)_3$ (x=0.01, x=0.04, and x=0.1) displayed on a logarithmic intensity scale at RT.

TABLE I. The luminescence decay properties of $Ba_3Gd_{1-x}Ce_x(BO_3)_3$.

Parameters (nm)	Doping concentration	Decay time (ns)
$\lambda_{ex}=345$, $\lambda_{em}=380$	0.01	$\tau_1=2.82$, $\tau_2=17.64$
	0.04	$\tau_1=3.18$, $\tau_2=16.04$
	0.10	$\tau_1=2.79$, $\tau_2=14.91$
$\lambda_{ex}=345$, $\lambda_{em}=520$	0.01	$\tau_1=2.35$, $\tau_2=19.45$
	0.04	$\tau_1=3.46$, $\tau_2=19.76$
	0.10	$\tau_1=2.82$, $\tau_2=22.21$
$\lambda_{ex}=370$, $\lambda_{em}=520$	0.04	$\tau_1=1.52$, $\tau_2=20.44$
	0.10	$\tau_1=1.94$, $\tau_2=22.54$

electric dipole allowed transition in Ce^{3+}. In this work, the lowest energy of the electric dipole allowed transition in $Ce^{3+}(1)$ is 28.8×10^3 cm^{-1} (347 nm) corresponding with $D(A)=20.5\times10^3$ cm^{-1}. Similarly $D(A)=22.0\times10^3$ cm^{-1} for $Ce^{3+}(2)$. $D(A)$ is a property that characterizes a compound, and its value does not depend on the type of lanthanide ion. Since the lowest energy of the $4f$-$5d$ transitions in the free ion Gd^{3+} is at 95 160 cm^{-1}, the Dorenbos expression predicts the $4f$-$5d$ transition with the lowest energy for $Gd^{3+}(1)$ or $Gd^{3+}(2)$ in $Ba_3Gd(BO_3)_3$ at around 135 nm which is clearly a too short wavelength to explain band H in Fig. 2.

The luminescence decay curves for $Ba_3Gd_{1-x}Ce_x(BO_3)_3$ for $x=0.01$, $x=0.04$, and $x=0.1$ at RT are shown in Fig. 8. The curves are well fitted by a sum of two exponential curves which provide with the values for two decay times τ_1 and τ_2 summarized in Table I. The decay time value for τ_1 is much shorter than the usual lifetime (20–60 ns) of the $5d$ state of Ce^{3+} in compounds. It indicates the presence of a luminescence quenching mechanism. Possibly the excitation energy of Ce^{3+} is transferred via the Gd sublattice to quenching sites. The about 20 ns decay time associated with τ_2 is more close to typical $5d$ lifetime of Ce^{3+}.

D. X-ray excited luminescence of $Ba_3Gd(BO_3)_3:Ce^{3+}$

The x-ray excited luminescence of $Ba_3Gd(BO_3)_3:0.04Ce^{3+}$ is shown in Fig. 9. The spectrum was measured under the same experimental conditions as that of a BaF_2 reference sample. The spectrum of $Ba_3Gd_{0.96}Ce_{0.04}(BO_3)_3$ shows a sharp emission at 313 nm due to $^6P_{7/2}$-^8S emission from Gd^{3+} and a broad emission band peaking at 418 nm attributed to Ce^{3+} $5d$-$4f$ emission. The shape of the emission band is similar to the emission excited by uv and vuv in Fig. 4. The only difference is that the x-ray excited emission is at slightly longer wavelength.

An estimate for the x-ray excited absolute light yield output of the sample of Fig. 9 was made from the ratio between its wavelength integrated emission intensity with that of the BaF_2 reference sample. With the methods outlined,[25] we found for our reference BaF_2 crystal a light output of about 9300 photons/MeV absorbed gamma ray energy. We obtain for the absolute yield of sample $Ba_3Gd(BO_3)_3:0.04Ce^{3+}$ about 370±30 photons/MeV. These are two orders of magnitude lower than the number of ionization created per 1 MeV of absorbed x-ray energy, and $Ba_3Gd(BO_3)_3:Ce^{3+}$ is a very poor x-ray phosphor.

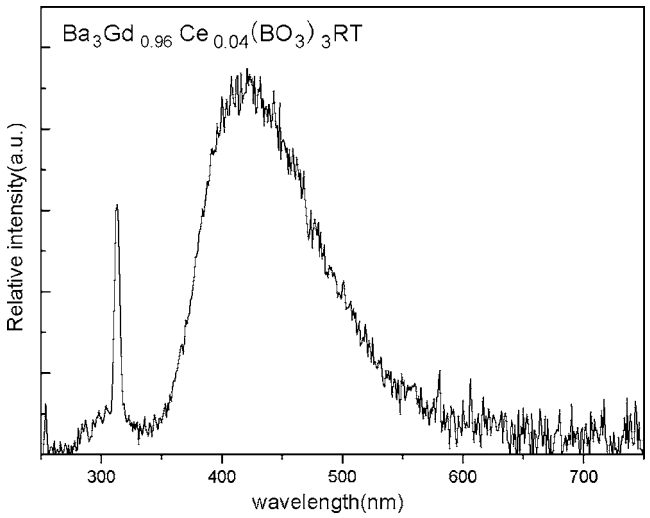

FIG. 9. X-ray excited emission spectrum of $Ba_3Gd(BO_3)_3:Ce^{3+}$ at room temperature.

IV. CONCLUSIONS

A series of phosphors with molecular formulas $Ba_3Gd_{1-x}Ce_x(BO_3)_3$ ($x=0$, 0.01, 0.02, 0.04, 0.06, 0.08, and 0.1) was synthesized by the method of solid-state reaction at high temperature. The spectroscopic properties in the vuv, uv, and visible range were investigated and discussed. The host-related absorption was found near 195 nm. It is found that Ce^{3+} ions preferentially enter the larger Gd(1) sites when the doping concentration is low. The occupancy probability of the smaller Gd(2) sites increases with increasing Ce^{3+} concentration in samples $Ba_3Gd_{1-x}Ce_x(BO_3)_3$. The x-ray excited emission spectra of $Ba_3Gd(BO_3)_3:Ce^{3+}$ was investigated but its light yield is very small and $Ba_3Gd(BO_3)_3:Ce^{3+}$ is a poor x-ray phosphor.

ACKNOWLEDGMENTS

The work is financially supported by the National Natural Science Foundation of China (Grant No. 20571088) and by the Science and Technology Project of Guangdong province (Grant No. 2006B14801001).

[1] P. Dorenbos, J. Lumin. **91**, 155 (2000).
[2] P. Dorenbos, J. Lumin. **91**, 91 (2000).
[3] P. Dorenbos, J. Andriessen, and C. W. E. van Eijk, J. Solid State Chem. **171**, 13 (2003).
[4] T. Jüstel, H. Nikol, and C. Ronda, Angew. Chem., Int. Ed. **37**, 3084 (1998).
[5] M. J. Weber, J. Lumin. **100**, 35 (2002).
[6] C. Dujardin *et al.*, J. Phys.: Condens. Matter **10**, 3061 (1998).
[7] R. T. Wegh, H. Donker, K. D. Oskam, and A. Meijerink, J. Lumin. **82**, 93 (1999).
[8] R. T. Wegh, E. V. D. van Loef, and A. Meijerink, J. Lumin. **90**, 111 (2000).
[9] J. R. Cox, D. A. Keszler, and J. F. Huang, Chem. Mater. **6**, 2008 (1994).
[10] T. N. Khamaganova, N. M. Kuperman, and Zh. G. Bazarova, J. Solid State Chem. **145**, 33 (1999).
[11] T. N. Khamaganova, N. M. Kuperman, and Zh. G. Bazarova, Zh. Neorg. Khim. **43**, 1100 (1998).
[12] T. N. Khamaganova and N. M. Khrushcheva, Russ. J. Appl. Chem. **78**, 23 (2005).
[13] S. K. Pan and G. F. Wang, Jiegou Huaxue (Chinese Journal of Structural Chemistry) **22**, 187 (2003).
[14] X. Z. Li, X. L. Chen, L. Wu, Y. G. Cao, T. Zhou, and Y. P. Xu, J. Alloys

Compd. **370**, 53 (2004).
[15]S. K. Pan and G. F. Wang, Jiegou Huaxue (Chinese Journal of Structural Chemistry) **22**, 550 (2003).
[16]X. Z. Li, X. L. Chen, J. K. Jian, L. Wu, Y. P. Xu, and Y. G. Cao, J. Solid State Chem. **177**, 216 (2004).
[17]Q. Zeng *et al.*, J. Phys.: Condens. Matter **18**, 9549 (2006).
[18]Z. F. Tian, H. B. Liang, H. H. Lin, Q. Su, B. Guo, G. B. Zhang, and Y. B. Fu, J. Solid State Chem. **179**, 1356 (2006).
[19]R. D. Shannon, Acta Crystallogr., Sect. A: Cryst. Phys., Diffr., Theor. Gen. Crystallogr. **32**, 751 (1976).
[20]C. J. Duan, J. L. Yuan, and J. T. Zhao, J. Solid State Chem. **178**, 3698 (2005).
[21]Y. H. Wang, T. Endo, E. Q. Xie, D. Y. He, and B. Liu, Microelectron. J. **35**, 357 (2004).
[22]P. Dorenbos, J. Phys.: Condens. Matter **15**, 8417 (2003).
[23]L. H. Tian, B. Yu, C. Pyun, H. L. Park, and S. Mho, Solid State Commun. **129**, 43 (2004).
[24]P. Dorenbos, J. Lumin. **111**, 89 (2005).
[25]J. T. M. de Haas, P. Dorenbos, and C. W. E. van Eijk, Nucl. Instrum. Methods Phys. Res. A **537**, 97 (2005).
[26]PDF No. 51-0425 (unpublished); PDF No. 51-0172 (unpublished); PDF No. 52-0373 (unpublished); PDF No. 51-1848 (unpublished); PDF No. 50-0098 (unpublished).